ACTIVE VORTICAL FLOW CONTROL FOR ALLEVIATION OF TWIN-TAIL BUFFET OF GENERIC FIGHTER AIRCRAFT

E. F. Sheta and V. J. Harrand

CFD Research Corporation, Huntsville, AL 35805, U.S.A.

and

L. J. Huttsell

AFRL, Wright Patterson AFB, Dayton, OH 45433, U.S.A.

A multidisciplinary computational investigation has been conducted to examine the feasibility of controlling the buffet problem using different active flow control methods. Tangential central blowing (TCB), tangential vortex blowing (TVB), and tangential spanwise blowing (TSB) methods were used to inject high-momentum fluid into the vortical flow of generic fighter aircraft flying at 30° angle of attack. The effect of blowing strength on the buffet responses is also investigated. The injection is aimed to strengthen the wing vortices and to delay the onset of breakdown in order to alleviate the twin-tail buffet. The results indicated that blowing directly into the core of the leading-edge vortices has more potential in controlling the buffet responses and in the reformation of unburst vortices with larger length. The TVB method produced the most favorable results with a reduction of about 43% in the buffet excitation parameter and a reduction of about 40% in the amplitude of bending deflection. This multidisciplinary investigation is conducted using the multidisciplinary computing environment (MDICE).   © 2001 Academic Press

1. INTRODUCTION

THE BUFFET PROBLEM is a multidisciplinary aeroelastic phenomenon that limits the performance of current and new generation of fighter aircraft. In buffet conditions, the vortices emanating from the sharp leading edges of the wing break down upstream of the vertical tails, as the case of the F/A-18 aircraft shown in Figure 1. The breakdown flow induces unsteady buffet loads on the vertical tails which lead to their premature fatigue failure, causing the USAF millions of dollars every year for inspections and repairs.

Experimental investigations of the vertical tail buffet of the F/A-18 models have been conducted by several investigators such as Sellers *et al.* (1988), Wentz (1987), Lee *et al.* (1990), and Cole *et al.* (1990). These experiments showed that the vortex produced by the LEX of the wing breaks down ahead of the vertical tails at angles of attack of 25° and higher producing unsteady loads on the vertical tails. The buffet response occurs in the first bending mode, increases with increasing dynamic pressure and is larger at $M = 0.3$ than that at higher Mach numbers. Washburn *et al.* (1993) conducted an extensive experimental investigation of the effect of twin-tail location on the buffet responses. They showed that as the tails were moved laterally toward the vortex core, the buffeting response and excitation were reduced. The aerodynamic loads were more sensitive to the chordwise tail location than its spanwise location.

Figure 1. Flow visualization of the F-18 HARV vortex breakdown ahead of the vertical tails. Photograph courtesy of the NASA Dryden Flight Research Center.

Numerical investigation of buffet problem has been conducted by Rizk *et al.* (1992) and Gee *et al.* (1995) for F/A-18 model, and by Findlay (1997) and Morton *et al.* (1998) for delta-wing/twin-tail model using Reynolds-averaged, thin-layer Navier–Stokes equations. A weak coupling between the structures and aerodynamics are considered in these studies by assuming only rigid tails. Thus, the inertial effects of the tail motion on the flow field were neglected. These effects have been shown by Washburn *et al.* (1993) to significantly affect the unsteady pressure loading on the tails. They concluded that the dominant frequency is very close to the first natural frequency of the tail. The tails were responding mainly in the first bending mode. Kandil *et al.* (1996, 1997), Kandil & Sheta (1997) and Sheta & Kandil (1999) conducted a series of strong-coupling numerical investigations on the twin-tail buffet using Reynolds-averaged, full Navier–Stokes equations. The oscillations of the tails were shown to affect the vortex breakdown locations and the unsteady aerodynamic loads on the wing and tails. A comprehensive discussion of these studies is presented by Sheta (1998).

The vortical flow associated with flow separation at the leading edges of a delta wing contributes significantly to the aerodynamic characteristics and to the dynamic loads on various parts of the aircraft. Several flow control methods might be used to alter the evolution of the vortical flow over the aircraft, or to alter the path of the vortices and the onset of breakdown. This is either to improve the aircraft performance or to alleviate vibrations of certain parts of the aircraft as in the case of twin-tail buffet problem. As a near-term solution to the buffet problem on the F/A-18 aircraft, a streamwise fence was fitted over the wing LEX with minimal understanding of the flow physics involved, see Lee & Valerio (1994) and Shah (1991). Shah (1991) showed that each leading-edge vortex is separated into two counter-rotating vortices, as it passes over the fence. These secondary vortices were generated outboard of the primary one and pulls some of its energy outboard, away from the tails. In addition, the vortex energy is dispersed over a larger region. In flight tests by Lee *et al.* (1990) without LEX fence, peak accelerations of $450g$ close to the tip of the vertical tail were measured. With the addition of LEX fences, the peak accelerations were reduced to $200g$. A loss of 2–3% of maximum lift was seen, since the fence disrupts the basic
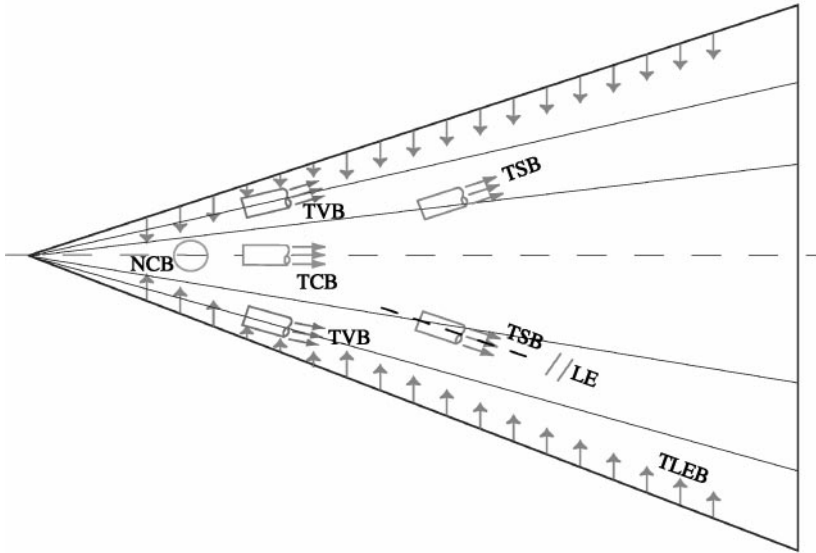
Figure 2. Schematic view of delta wing showing potential applications of jet blowing to improve the vortical flow characteristics. TSB: tangential spanwise blowing; TCB: tangential central blowing; TVB: tangential vortex blowing; TLEB: tangential leading-edge blowing; NCB: normal central blowing.

vortical flow. The fences were also less effective at high angles of attack as shown by Shah (1991), Lee *et al.* (1990), and Meyn & James (1993).

Some attempts have been made by Wong *et al.* (1994) and Wood & Roberts (1988) to control the leading-edge vortices using tangential leading-edge blowing (TLEB), see Figure 2. The TLEB is aimed to delay flow separation around rounded edges, and consequently the vortex breakdown by the means of Coanda effect. The Coanda effect caused the tangentially exiting jet to remain attached around the rounded surface at the leading edge. TLEB partially reattaches the flow around the leading edge, allowing the formation of a strong leading-edge vortex, and consequently effectively delaying the vortex breakdown. However, for sharp leading-edge wings (as the case of fighter aircraft) the Coanda effect is limited, as the primary flow separation cannot be prevented from happening at the leading edge.

Some experimental work by Anglin & Satran (1980) and Seginer & Salomon (1986) have shown that blowing a discrete spanwise jet (TSB) over the upper surface of a delta wing in a direction essentially parallel to the leading edge enhances the leading-edge vortex and delays the vortex breakdown to higher angles of attack with a substantial increase in lift. Anglin & Satran (1980) have investigated three positions of jet ports at 20, 30 and 40% chord stations. Only one port was used at a time. The investigation showed enhancement in vortex lift and increased the maximum lift coefficient. Use of blowing helped also eliminate a wing rock exhibited in the basic configuration at about 20° angle of attack.

Apex jet blowing is another attempt for delaying vortex breakdown and improving the aerodynamic performance of delta wings. Miller & Gile (1993) have introduced a blowing jet at the 10% chord station over 60 and 76°-sweep delta wings. Two blowing positions and directions were examined: centerline blowing (TCB) and vortex line blowing (TVB). In the centerline blowing, the jet blew along the model centerline. In the vortex line blowing, the jet blew in a direction parallel to the leading-edge vortex. In both cases, the jet was positioned to blow tangent to the wing upper surface. The investigation revealed that the blowing

direction on the 60°-sweep wing and the blowing rate on the 76°-sweep wing have the greatest effect on vortex behavior and its breakdown. Blowing parallel to the 60°-sweep wing vortex core and blowing along the 76°-sweep wing centerline at the highest rate provided the greatest delay in the vortex breakdown location.

Sheta *et al.* (1998) and Sheta & Kandil (1999) conducted a numerical investigation on the use of flow suction along the vortex cores (FSVC) and TLEB to control twin-tail buffet. The TLEB produced lower tail root-bending moment, torsion deflection and acceleration. However, the bending deflection and acceleration were higher than those of the no-control case. The FSVC method reduced the bending deflection. However, the RBM, bending and torsion accelerations were higher than those of the no-control case. The combined effect and the effect of suction angle were also investigated.

In collaboration with the AFRL, an extensive computational investigation is currently ongoing to examine the feasibility of controlling the tail buffeting using flow and structure control. In the current paper, some of the findings and lessons learned from the active flow control of the twin-tail buffet are presented. Tangential central blowing (TCB), tangential vortex blowing (TVB), and tangential spanwise blowing (TSB) were applied to a generic twin-tail fighter aircraft to alleviate the buffet. This complex multidisciplinary problem is performed using the multidisciplinary computing environment (MDICE), see Kingsley *et al.* (1998).

MDICE provides an environment in which several engineering analysis modules run concurrently and cooperatively to perform complex multidisciplinary applications. Using MDICE, inherently dissimilar disciplines and programs from a variety of sources, written in different computer languages, for different grid structures, can be coupled and synchronized to run over a distributed heterogeneous network of computers (DEC, SGI, SUN, NT). Those codes or modules may perform distinct tasks such as fluid-structural analysis, geometry modeling, controls and multidisciplinary design. A large number of commercial, research, U.S. Government, and public domain codes have already been integrated into the MDICE environment. Examples of these codes are Pro-Engineer, Unigraphics, CATIA, MSC-NASTRAN, Cobalt (AFRL), NPARC (NASA LeRC), ADPAC (NASA LeRC), Split-flow (Lockheed Martin), GCNS (Northrop Grumman), CFD-FASTRAN, CFD-ACE, and CFD-FEMSTRESS (CFDRC).

2. MDICE ARCHITECTURE

MDICE is a distributed object-oriented environment, which is made up of several major components. The first component in an MDICE is a central controlling process that provides network and application control, serves as an object repository, carries out remote procedure calls, and coordinates the execution of the several application programs via MDICE specific script language. The second component is a collection of libraries, each containing a set of functions callable by the application programs. These libraries provide low-level communication and control functions that are hidden from the application programs, as well as more visible functionality such as object creation and manipulation, interpolation of flow data along interfaces, and safe dynamic memory allocation services. Finally, the environment also encompasses a comprehensive set of MDICE compliant application programs. MDICE provides capabilities for parallel execution of participating application programs and has a full interface for those codes written in Fortran 77 or 90, C, or C++.

In the application control panel of MDICE, the application modules are selected. For each module, the computer host or hosts are chosen. Other information is provided, such as specifying a directory to run each module and any command line arguments the module

might require. Once the simulation has been set up, it is run and controlled by MDICE using a short script in the graphical user interface (GUI). The MDICE GUI explicitly specifies the synchronization between the modules. The MDICE script contains all the conveniences found in most common script languages. In addition, MDICE script supports remote procedure calls and parallel execution of the application modules. These remote procedure calls are the mechanism by which MDICE controls the execution and synchronization of the participating applications. Each application posts a set of available functions and subroutines. These functions are invoked from MDICE script, but are executed by the application program which posted the function.

There are many advantages to the MDICE approach. Using this environment, one can avoid giant monolithic codes that attempt to provide all the needed services in a single large computer program. Such large programs are difficult to develop and maintain and by their nature cannot contain up-to-date technology. The MDICE allows the reuse of existing, state-of-the-art codes that have been validated. The flexibility of exchanging one application program for another enables each engineer to select and apply the technology best suited to the task at hand. Efficiency is achieved by utilizing a parallel-distributed network of computers. Extensibility is provided by allowing additional engineering programs and disciplines to be added, without modifying or breaking the modules or disciplines already in the environment. For more details of MDICE architecture, see Kingsley *et al.* (1998).

3. MULTIDISCIPLINARY AEROELASTIC APPLICATION OF CONTROL OF TWIN-TAIL BUFFET VIA MDICE

The application of MDICE computing environment to control the aeroelastic twin-tail buffet problem involves four types of modular functionality: fluid–dynamics module, fluid–structure and fluid–fluid interfacing module, structural dynamics module, and grid motion module. Next, the particular set of analysis modules used for the buffet simulation is presented, followed by the description of the generic fighter aircraft and the characteristics of flow control methods.

3.1. Fluid-Dynamics Module

The fluid–dynamics analysis module used for the current study is CFD-FASTRAN, CFDRC (1998). CFD-FASTRAN is a full Navier–Stokes flow solver for modeling compressible, turbulent flow problems using structured and/or unstructured grids. The solution of full Navier–Stokes equations is crucial for this problem to account accurately for the massive three-dimensional separations, vortex breakdown and vorticity evolution, convection and shedding, and strong fluid–structure interaction. CFD-FASTRAN employs an upwind scheme with Roe's flux-difference splitting or Van-Leer's flux-vector splitting for spatial differencing. Temporal differencing is done using a Runge–Kutta scheme, a point-implicit scheme or a fully implicit scheme. Turbulent models in CFD-FASTRAN include Baldwin-Lomax, Spalart-Allmaras, k–ε, and k–ω models. CFD-FASTRAN also provides modeling for flow problems with multiple moving bodies using automated Chimera overset gridding methodology coupled with a 6DOF model. The current simulation used a fully implicit scheme with Roe's flux-difference splitting.

The physical boundary conditions assume that the flow field is in an undisturbed free-stream state at an infinite distance from the wing and tails in all directions. On the wing and tails surfaces, the no-slip and no-penetration conditions are enforced, that is the relative velocity must be equal to zero. The normal pressure gradient is equal to zero on stationary surfaces. On the accelerating tail surfaces, the normal pressure gradient is no longer equal to

zero due to the acceleration of the grid points. The normal pressure gradient becomes $\partial p/\partial \hat{\mathbf{n}} = - \rho(\mathbf{a} \cdot \hat{\mathbf{n}})$ on moving bodies, where $\mathbf{a}$ is the acceleration of a point on the accelerating surface and $\hat{\mathbf{n}}$ the unit normal. The temperature is enforced at the solid surfaces using adiabatic boundary conditions.

3.2. STRUCTURAL-DYNAMICS MODULE

The current structural-dynamics modules, which are MDICE compliant, include the nonlinear FEM code MSC/NASTRAN, CFDRC's FEM code FEMSTRESS, and MDICE's own structural interface. The MDICE structural-interface includes capabilities for various linear structural simulation models, such as the influence coefficient, modal analysis, and beam models. In the current analysis, the beam model of the MDICE structural interface is used. The vertical tails are modeled as cantilevered beams fixed at the root. The tail bending and torsional deflections occur about an elastic axis that is displaced from the inertial axis. The equations for the bending deflection, w, and the torsion deflection, θ, are given by

$$\frac{\partial^2}{\partial z^2}\left[EI(z)\,\frac{\partial^2}{\partial z^2}\,w(z,t)\right] + m(z)\,\frac{\partial^2}{\partial t^2}\,w(z,t) + m(z)\,x_\theta\,(z)\,\frac{\partial^2}{\partial t^2}\,\theta(z,t) = N(z,t), \qquad (1)$$

$$\frac{\partial}{\partial z}\left[GJ(z)\,\frac{\partial}{\partial z}\,\theta(z,t)\right] - m(z)x_\theta(z)\,\frac{\partial^2}{\partial t^2}\,w(z,t) - I_\theta(z)\,\frac{\partial^2}{\partial t^2}\,\theta(z,t) = -M(z,t), \qquad (2)$$

where z is the vertical distance from the tail-root fixed support, $EI(z)$ and $GJ(z)$ are the bending and torsional stiffness of the tail section, $m(z)$ the mass per unit length, I_θ is the mass moment of inertia per unit length about the elastic axis, x_θ the distance between the elastic axis and the inertia axis, N and M are the normal force and twisting moment per unit length. The geometric and natural boundary conditions on w and θ are given by

$$w(0, t) = \frac{\partial}{\partial z}\,w(0, t) = 0, \qquad (3)$$

$$\frac{\partial^2}{\partial z^2}\,w(h, t) = \frac{\partial}{\partial z}\left[EI(h)\,\frac{\partial^2}{\partial z^2}\,w(h, t)\right] = 0, \qquad (4)$$

$$\theta(0, t) = \frac{\partial}{\partial z}\,\theta(h, t) = 0. \qquad (5)$$

The equations are transformed into a set of coupled second-order ODEs using the Galerkin method and modal analysis. The resulting aeroelastic equations are solved using a fifth-order accurate Runge–Kutta scheme. Details of the aeroelastic equations and their solution procedure are presented by Sheta (1998).

3.3. FLUID–STRUCTURE INTERACTION MODULE

The fluid–structure interface algorithm is used to project the forces and moments from the fluid flow to the flexible-body structure and to feed back the aeroelastic deflections of the structure to the flow field. The interfacing is formulated in the most general sense for maximum flexibility. There are no inherent assumptions that the fluids grid is matched with the structure grid, either through different mesh densities, mesh architecture, or through physical separation between the interfaces, as seen in the thick-shell finite-element models. The current simulation uses a conservative and consistent interface adapted from Brown

(1997). Conservative interfaces aim to conserve the forces and moments in the interpolation process between two grids. In this case, the sum of all forces and moments on the fluid interface is equivalent to the sum of all forces and moments on the structure interface, i.e.,

$$\sum_{\text{fluidfaces}} \mathbf{F}_{\text{fluid}} = \sum_{\text{solidnodes}} \mathbf{F}_{\text{solid}}, \tag{6}$$

$$\sum_{\text{fluidfaces}} \mathbf{M}_{\text{fluid}} = \sum_{\text{solidnodes}} \mathbf{M}_{\text{solid}}. \tag{7}$$

Consistency (virtual work conservation) requires that the virtual work performed by the solid interface, W_{solid}, is equivalent to the virtual work performed by the fluid interface, W_{fluid}, i.e.,

$$\sum_{\text{fluidfaces}} \mathbf{W}_{\text{fluid}} = \sum_{\text{solidnodes}} \mathbf{W}_{\text{solid}}, \tag{8}$$

$$\mathbf{W}_{\text{fluid}} = \mathbf{F}_{\text{fluid}} \cdot \Delta \mathbf{r}_{\text{center}}, \tag{9}$$

$$\mathbf{W}_{\text{solid}} = \mathbf{F}_{\text{solid}} \cdot \Delta \mathbf{x} + \mathbf{M}_{\text{solid}} \cdot \omega_{\text{solid}}. \tag{10}$$

These equations apply only to the degrees of freedom of the structure-dynamics equations. The MDICE environment contains many types of function-matching interfaces and conservative interfaces techniques. For more details, see Siegel *et al.* (1998).

3.4. GRID MOTION MODULE

At every time step, the grid is deformed to accommodate the deformed tails. The six outer boundary surfaces of the computational domain are kept fixed. The grid is deformed using the transfinite interpolation functions (TFI), see Thompson *et al.* (1998). The advantage of using TFI is that TFI is an interpolation procedure that deforms grids conforming to specified boundaries and it is computationally very efficient. The spacing between points in the physical domain is controlled by blending functions that specify how far the effect of the new position of the flexible body surfaces is carried into the original grid. The grid points near the surface of the tails are moving with the tails. The motion of the grid points decreases as one goes far from the boundary in all directions, and vanishes at the outer boundary of the deformed block. The TFI routine is invoked automatically when a fluid–structure interface is exchanged between application modules.

3.5. GENERIC FIGHTER AIRCRAFT

In the current study, a generic model of fighter aircraft is chosen to study the effect of different flow control methodologies on twin-tail buffet. The configuration model consists of a $76°$-swept-back, sharp-edged delta wing of aspect ratio of 1 and dynamically scaled, flexible, swept-back twin tail of aspect ratio of 1·4, shaped after Washburn *et al.* (1993). The delta wing is identical to the geometry used by Hummel (1978) and has a sharp leading edge, a flat upper surface, and a triangular cross-section. The root chord of the wing is 1·5 ft (1 ft = 0·3048 m) and the maximum thickness is 2·1% of the root chord at 90% chord station. The vertical tails are oriented normal to the upper surface of the delta wing and have a leading-edge sweep of $62·5°$. The separation distance between the twin tail is 78% of the wing span. Each tail is modeled as a single aluminum spar and balsa wood covering, as shown in Figure 3. The aluminum spar has a taper ratio of 0·3 and is constructed from 6061-T6 alloys. The balsa-wood covering has a taper ratio of 0·23 and aspect ratio of 1·4.
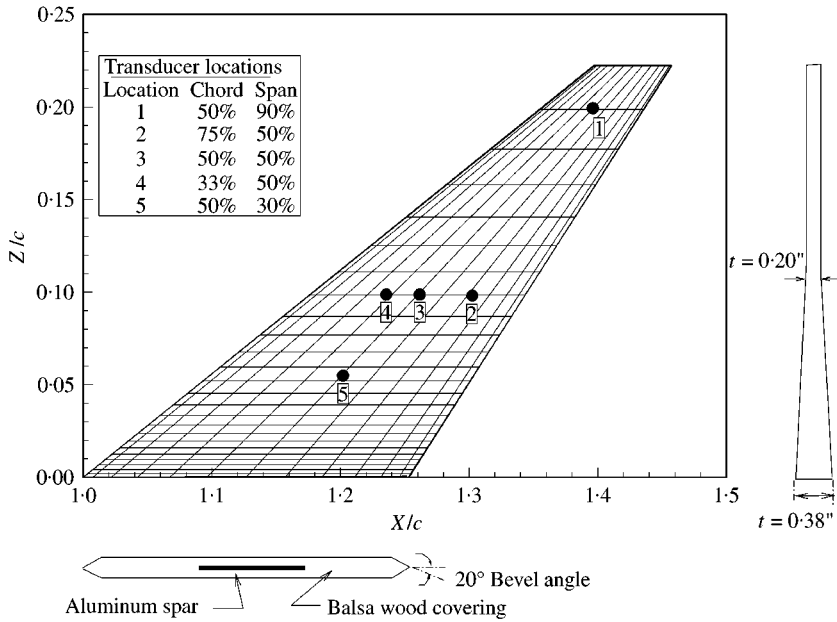
Figure 3. Schematic view of the vertical tail construction and dimensions; ( )″: in, where 1 in = 25·4 mm.
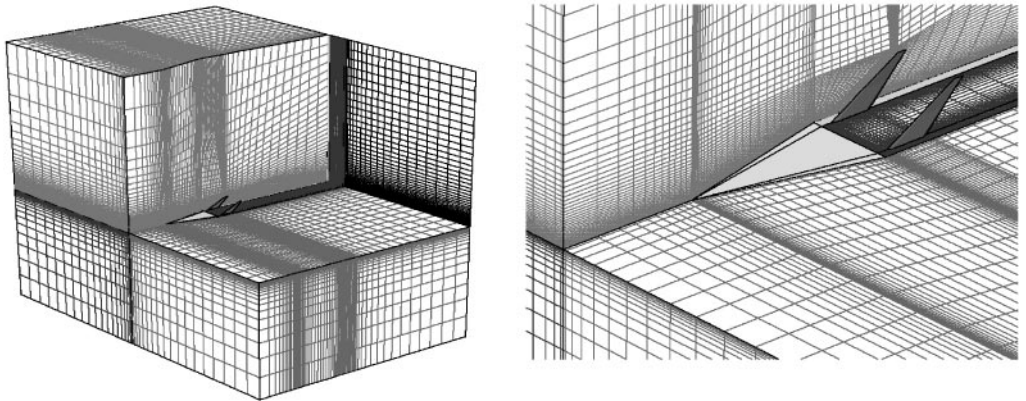
Figure 4. Three-dimensional and close-up views of the grid topology.

The details of the configuration model and the material properties are discussed in detail in Sheta (1998). The computational grid used in this study is shown in Figure 4. The grid is a multiblock H–H grid structure consisting of 11 blocks, C°-continuous, with a total size of 450 000 grid points. The delta-wing/twin-tail configuration is statically pitched to 30° angle of attack at Mach number of 0·4 and Reynolds number of $1·25 \times 10^6$.

3.6. FLOW CONTROL METHODS

The tangential central blowing (TCB), tangential vortex blowing (TVB), and tangential spanwise blowing (TSB) methods are considered in this paper to inject high momentum fluid into the vortical flow of the generic fighter aircraft. The effect of physical existence of

the blowing device is not modeled in this investigation. Only the effect of the blowing jet is considered. In these methods, a hypothetical jet is introduced at the 10% chord station over the delta wing, see Figure 2. The jets are directed to blow in a direction parallel and tangent to the wing surface. In the TCB method, the jet area is 43 mm^2. The jet is positioned at the wing center and blows along the wing centerline. In the TVB method, two jet tubes with an area of 27 mm^2 were positioned underneath the leading-edge vortices at the 10% chord station, and blow in a direction parallel to the wing leading-edge vortices. In the TSB method, two jet tubes with an area of 27 mm^2 were positioned underneath the leading-edge vortices at the 10% chord station, and blow in a direction essentially parallel to the leading edges of the wing.

The jet is simulated numerically by defining a permeable boundary, corresponding to the jet slot, where inlet-flow boundary conditions are implemented. At the jet-exit boundary, the flow density is assumed constant and equals to 3·5 times the free-stream value, see Anglin & Satran (1980). The pressure is extrapolated and the temperature is fixed at the free-stream value. The jet exit velocity, V_j, is computed from a specified blowing strength, C_T.

$$C_T = (m_j V_j)/(q_\infty S), \qquad (11)$$

where m_j is the jet mass flow rate, q_∞ the free-stream dynamic pressure, S and the wing surface area. The maximum jet exit velocity is limited to Mach number of 0·6 to prevent supersonic blowing. Four blowing strengths were investigated: 0·002, 0·005, 0·008, and 0·01.

4. RESULTS AND DISCUSSION

This multidisciplinary aeroelastic problem is solved using two steps: the first step solves for the steady-state solution around the rigid configuration. The initial condition of this step corresponds to the undisturbed free-stream condition. The solution is carried out until the changes of the vortical flow field above the configuration becomes very small. The second step solves for the aerodynamic flow and aeroelastic responses of the flexible tails. The initial condition of this step is the final solution of step one. The time steps of the rigid and flexible computations are 10^{-4} s. The delta-wing/twin-tail configuration is statically pitched to $30°$ angle of attack at Mach number of 0·4 and Reynolds number of $1·25 \times 10^6$. This multidisciplinary problem is solved on a computer cluster consisting of four DEC ALPHA 500 Mhz units using the multidisciplinary computing environment (MDICE).

The simulation panel of the multidisciplinary computing environment (MDICE) is shown in Figure 5 for the aeroelastic twin-tail buffet simulation of generic fighter aircraft. The MDICE script is shown in the background of the figure. A snapshot of the total pressure isosurfaces over the configuration model is displayed over the simulation panel. Also shown are histories of the right-tail-tip bending and torsional deflections and right-tail-root bending moment. These images are graphically displayed in conjunction with MDICE GUI and can be invoked from MDICE as separate display modules. The aeroelastic results of the twin-tail buffet of the basic configuration (no blowing) have been extensively computed over a wide range of angles of attack, see Sheta *et al.* (1999). The results have been validated using the experimental data of Washburn *et al.* (1993). There were two distinct frequency peaks in the frequency band of the buffet excitation spectra. These peaks represent coherent fluctuations in the flow at those frequencies. The variations of these two distinct frequencies (n_1 and n_2) for the inner tail-tip point versus the angle of attack are shown in Figure 6. The nondimensional frequency is defined as ($n = fb/U_\infty$), where f is the frequency in Hz, b the wing span, and U_∞ the free-stream velocity. Figure 6 also shows the variation of the r.m.s. of the right-tail root-bending moment versus the angle of attack. The
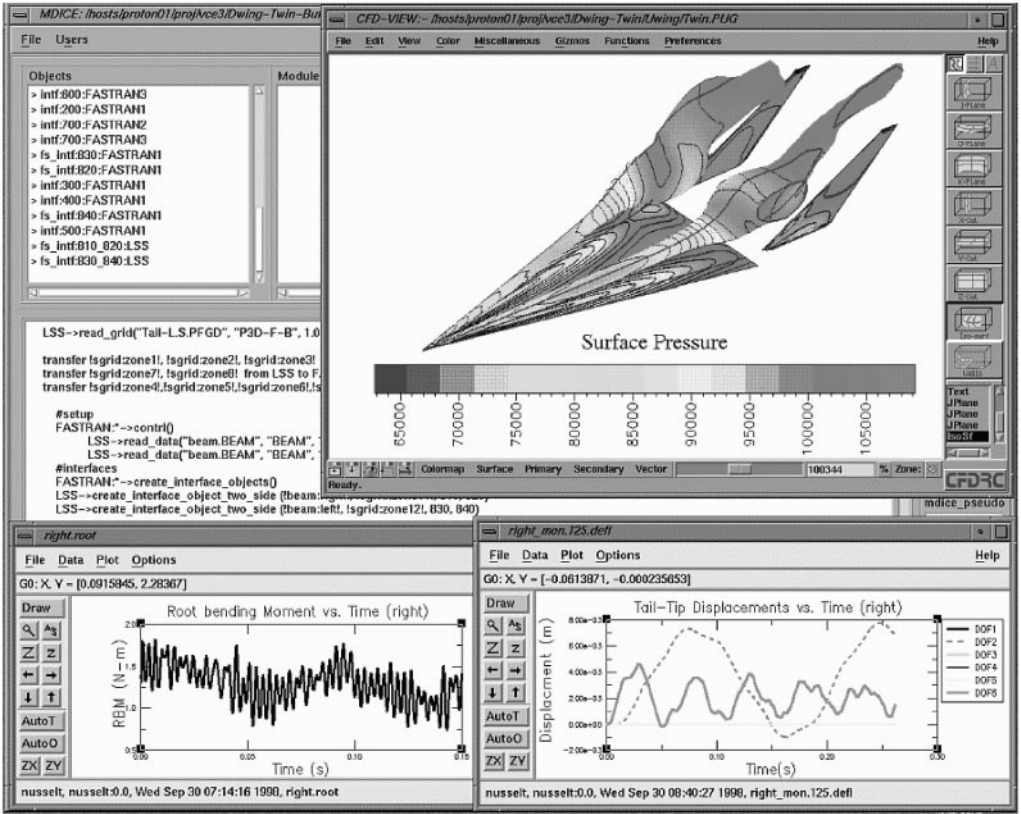
Figure 5. Simulation panel of the multidisciplinary computing environment (MDICE) showing the aeroelastic twin-tail buffet simulation of generic fighter aircraft.
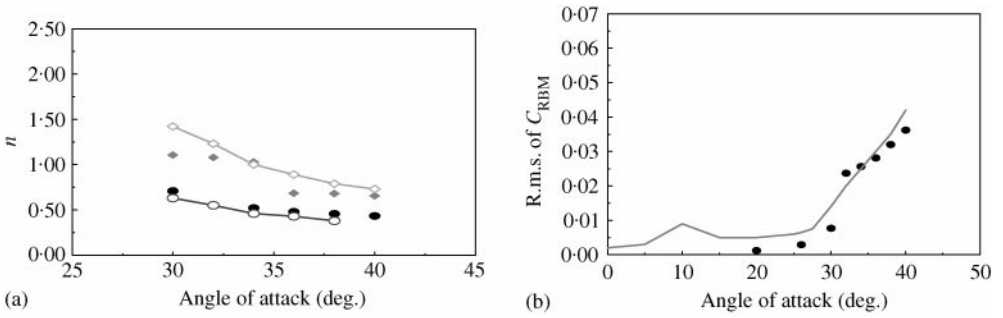
Figure 6. Nondimensional predominant frequencies of inner-tail-tip point and the r.m.s. of the root-bending moment, compared with the experimental data of Washburn *et al.* (1993): (a) nondimensional frequencies; and (b) r.m.s. of root-bending moment. ●, n_1(MDICE); ◆, n_2(MDICE); ○—○, n_1(Experimental); ◇—◇, n_2(Experimental); ●, MDIC; ——, Experimental.

experimental data of Washburn *et al.* is also shown in the figure. The results are in good agreement with the experimental data. The frequency peaks shift to a lower frequency as the angle of attack increases. The first two frequencies are moderately close to each other, which indicates that the pressure field contains energy over a narrow frequency band. This is in agreement with the observations of Washburn *et al.* (1993) and Martin & Thompson (1991).
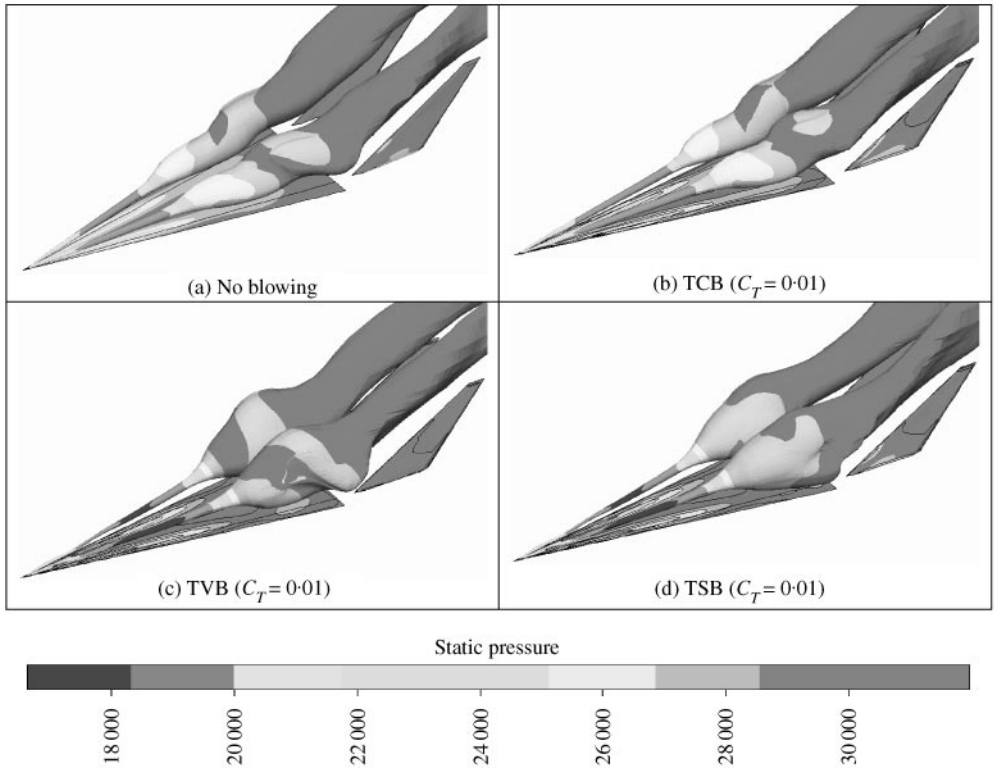
Figure 7. Three-dimensional perspective-view snapshots of the total-pressure isosurfaces.

The r.m.s. of the root bending moment experiences a sharp increase at the angle of attack of 25° and higher due to the upstream motion of the vortex breakdown flow in front of the twin tails. The difference between the numerical results and the experimental data at some points is attributed to the fact that the experiments were conducted using one rigid and one flexible tail, and the tails were supported using cylindrical steel booms, see Washburn *et al.* (1993). In the numerical simulations, the two tails are assumed to be flexible and suspended. An extensive validation of the computational results using the experimental data of Washburn *et al.* (1993) for the no-blowing case has been presented by Sheta *et al.* (1999) and Sheta (2000).

4.1. INSTANTANEOUS FLOWFIELD ANALYSIS

Figures 7 and 8 show three-dimensional and front view instantaneous snapshots of the total pressure isosurfaces over the configuration model, at time = 0·1 s, for the no-blowing case and for the different blowing methods at a blowing strength of 0·01. The figure shows that all blowing methods were successful in delaying the onset of vortex breakdown. This is more obvious in the TVB and TSB methods. The onset of vortex breakdown for the no-blowing case is at the 51% chord station. The onset of vortex breakdown moves downstream to the 60, 70, and 70·5% chord stations for the TCB, TVB, and TSB methods, respectively. It was observed that the onset of vortex breakdown moves back-and-forth within 5% of the chord station as discussed by Sheta (1998). Sheta (1998) also discussed the effect of angle of attack on the onset of vortex breakdown. Delaying the vortex breakdown resulted in a stronger vortex and stronger breakdown, as shown in the figures. In all cases, the leading-edge
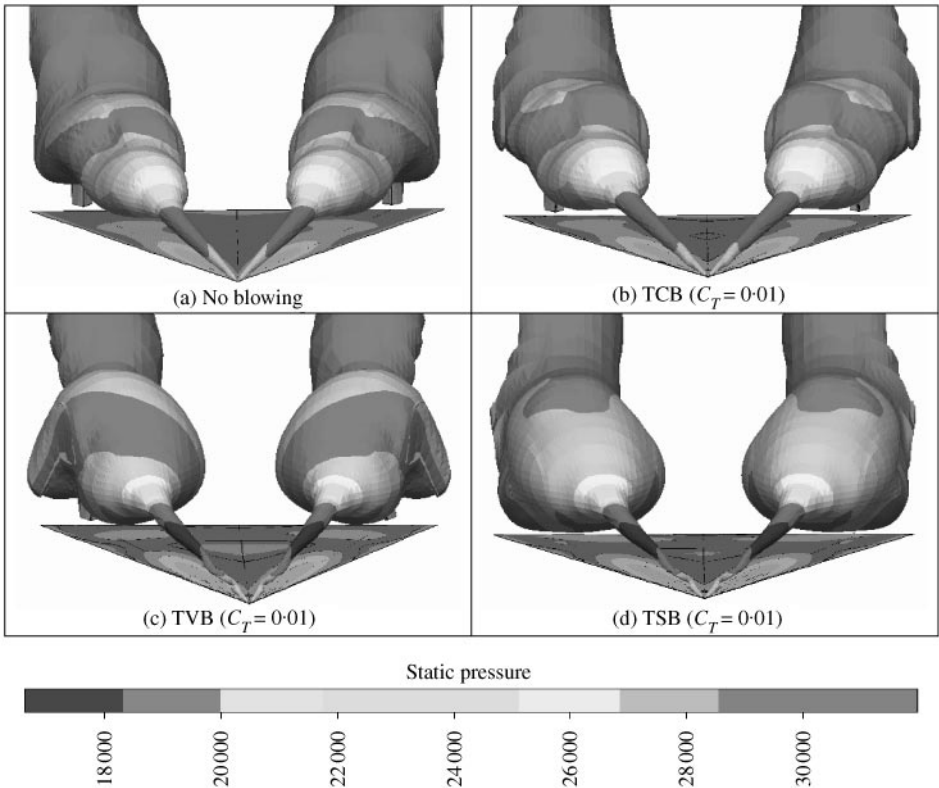
Figure 8. Front-view snapshots of the total-pressure isosurfaces.

vortices break down upstream of the twin tail. The tails cut through the center of the vortex breakdown flow. Figure 9 shows the distribution of the coefficient of pressure at different chord stations for the blowing cases (blowing strength of 0·01) compared to the no-blowing case. At the 30% chord station, much before the vortex breakdown, the figure shows strong suction peaks corresponding to the center of the primary vortex. As the flow travels downstream to the 50% chord station, the blowing cases show stronger suction peaks corresponding to the stronger leading-edge vortices. At the 90% chord station, far beyond the vortex breakdown, the blowing cases still show stronger vortices and suction peaks compared to the no-blowing case.

4.2. AEROELASTIC BUFFET LOADING AND RESPONSES

Figure 10 shows the buffet excitation spectra on both sides of the right tail at near-tip point (50% chord and 90% span). The buffet excitation parameter is defined as the nondimensional r.m.s. pressure parameter $\sqrt{nF(n)}$, where $F(n)$ is the contribution to power spectrum of $\bar{p}^2/q_\infty^2$ in a frequency band Δn, and n is the nondimensional frequency. The blowing cases did not alter the dominant frequencies. However, all the blowing cases have produced lower peaks (lower buffet excitation) than the no-blowing case. The TVB method produced the lowest buffet excitation peaks in all cases. The inner-surface primary buffet excitation peak is reduced by about 43%. The outer-surface primary peak reduced by about 10%. The
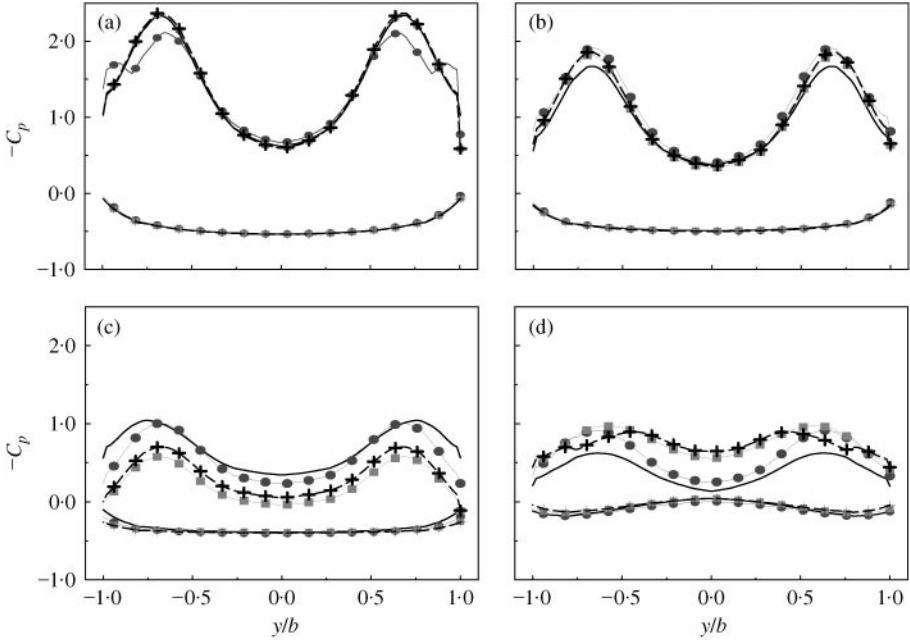
Figure 9. Distribution of coefficient of pressure, C_p, on the wing upper and lower surfaces at different chord stations: (a) at 30% chord station; (b) at 50%; (c) at 70%; (d) at 90% chord station. —, no blowing; ●—●, TCB ($C_T = 0{\cdot}01$); ■—■, TVB ($C_T = 0{\cdot}01$); +- + , TSB, ($C_T = 0{\cdot}01$).
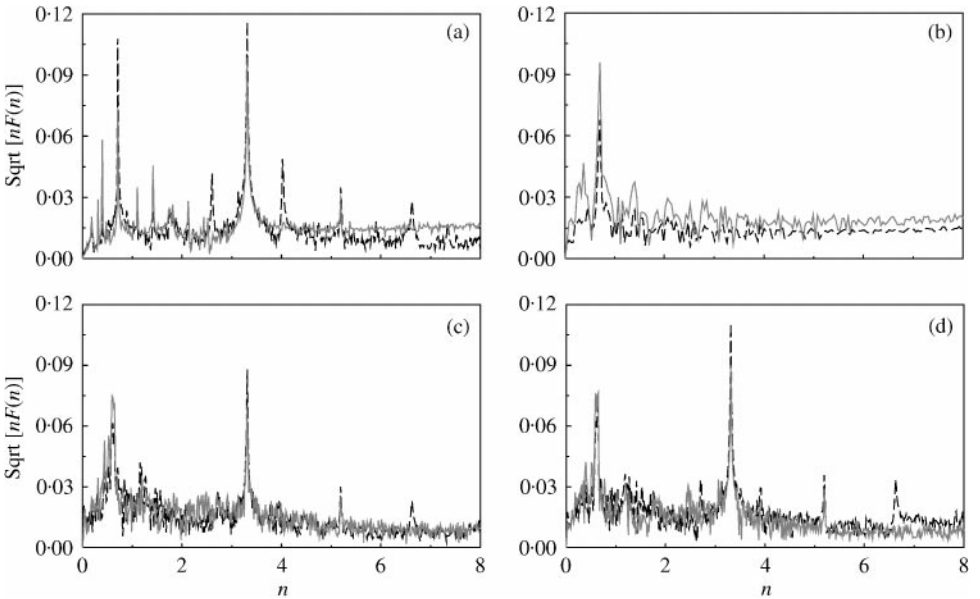
Figure 10. Buffet excitation parameter on the inner and outer surfaces of the right-tail tip (50% chord and 90% span): (a) no blowing; (b) TCB; (c) TVB; (d)TSB. – – –, inner surface; ——, outer surface.

largest buffet excitation peak, which occur at nondimensional frequency of 3·3, reduced by about 24%.

Figures 11 and 12 show the histories and power spectral density (PSD) of the root bending moment coefficient of the right and left tails at blowing strength of 0·01, compared
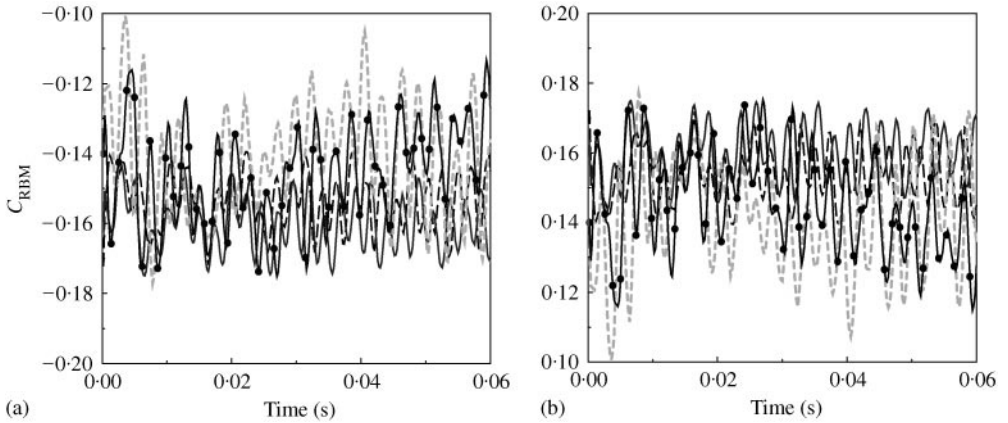
Figure 11. History of the root bending moment coefficient of (a) the left and (b) right tail: – – –, no blowing; — TCB ($C_T = 0.01$); ---, (faint line), TVB ($C_T = 0.01$); ●—●, TSB ($C_T = 0.01$).
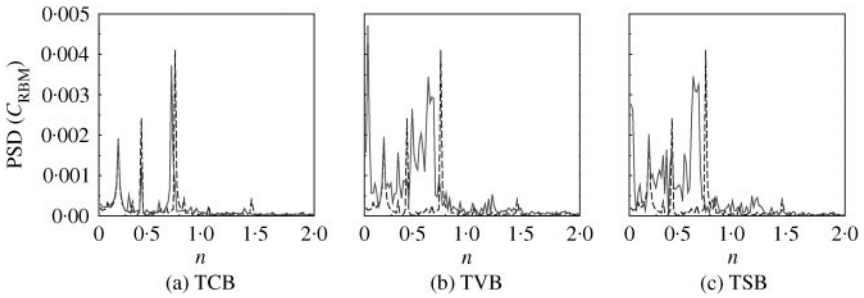
Figure 12. Power spectral density of the right-tail root bending moment for (a) TCB, (b) TVB, and (c) TSB: – – –, no blowing; —, with blowing ($C_T = 0.01$).

with the no-blowing case. The time domain is converted to the frequency domain using fast Fourier transform (FFT) technique. The MATLAB signal processing toolbox is used to perform the computations. Positive moments correspond to an outward force on the right tail. The figure shows that the two tails experience an outward bending force. This shows that the primary vortex flow passing outboard of the two tails produced stronger suction than that on the inboard of the tails. The figure also shows that the TVB and TSB methods have produced lower bending moments and PSD on both the right and left tails. However, the amplitude of oscillations is higher than that of the no-blowing case. The TVB method produced about 16·5% reduction in the largest PSD peak, while the TSB method produced about 15·5% reduction. Figure 13 shows the effect of blowing strength on the mean and r.m.s. of root bending moment coefficients. The figure shows that the TVB and TSB methods produced the lowest mean root bending moment, especially at blowing strength of 0·01. However, the r.m.s. of both is higher than that of the TCB method due to the large amplitude of load oscillations shown in Figure 11. Figures 10–13 clearly show that blowing directly toward the core of the leading-edge vortices has more potential in controlling the buffet loads, than blowing toward the center of the wing.

Figure 14 shows the effect of the blowing strength on the histories of the bending deflections of the right tail for the TCB, TVB, and TSB methods, respectively, compared
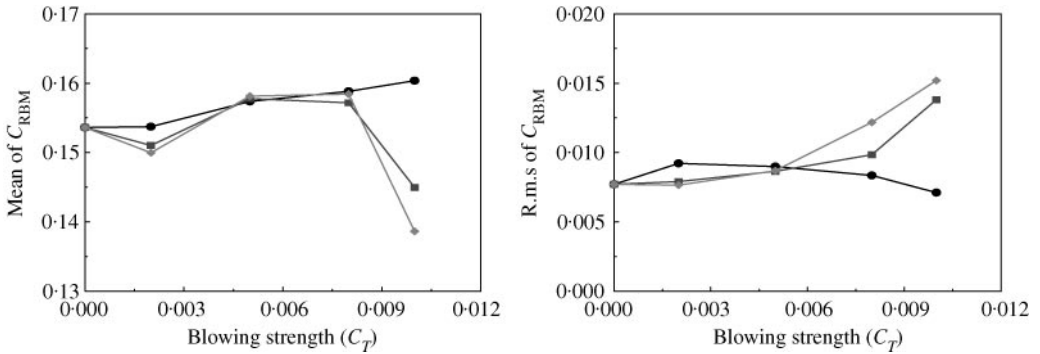
Figure 13. Effect of blowing strength on the right-tail mean and r.m.s. root bending moment coefficients: ●—●, TCB; ■—■, TVB; ◆—◆, TSB.

with the no-blowing case. In all cases, the amplitude of the bending deflections is effectively reduced by the blowing and the reduction increases with the increase in blowing strength. It is also observed that the high-frequency oscillations have reduced into sub-harmonic oscillations. The right tail is only moving toward the outboard direction. This is due to the outward bending forces observed in Figure 11.

Figure 15 shows the histories of the right-tail-tip bending deflections at a blowing strength of 0·01, compared with the no-blowing case. The figure shows a reduction of about 30–45% in the amplitude of bending deflections due to blowing. The TVB method produced the largest reduction followed by the TSB method. The figure also shows that the blowing methods produced a nearly damping bending response. Figure 16 shows the histories of the right-tail-tip torsional deflections at a blowing strength of 0·01, compared with the no-blowing case. The TVB and TSB methods produced almost the same response as that of the no-blowing case. However, the TCB method produced slightly larger amplitude than that of the no-blowing condition. The frequency of the torsion deflections is more than twice the frequency of the bending deflections, in agreement with the experimental observations. The figure also shows an increase in the amplitude of deflection with time. However, the rate of increase slows down with time due to the coupling with the bending mode of oscillations, which show a nearly damping response. Since the response of the torsional deflection at 30° angle of attack was very interesting, the responses at different angles of attack (26, 34 and 38°) were computed and shown in Figure 17 for the no-blowing case. Figures 16 and 17 show that the torsional deflection increases only at 30° angle of attack. This might be attributed to the location of vortex breakdown. At 26° angle of attack, the onset of vortex breakdown was very close to the wing trailing edge and apparently the vortex-breakdown flow did not interact fully with the tails (Sheta, 2000). At 34 and 38° angles of attack, the onset of vortex breakdown was near the apex of the wing and the vortex breakdown flow experienced some dissipation before interacting with the tails (Sheta, 2000).

Figure 18 shows the power spectral density of the bending and torsional accelerations of the right-tail tip at a blowing strength of 0·01, compared with the no-blowing case. The TSB method produced about a 90% reduction in the PSD of the first peak of the bending acceleration, compared to 82% in the TVB and TCB methods. However, the TVB produced about 44% reduction in the PSD of the second peak, compared to 12·5% in the TSB method and 7% in the TCB method. On the other hand, the TVB method produced about 55% reduction in the PSD of the largest peak in the torsion acceleration, compared to an increase of about 4% with the TSB. Figures 14–18 support the conclusion given earlier that
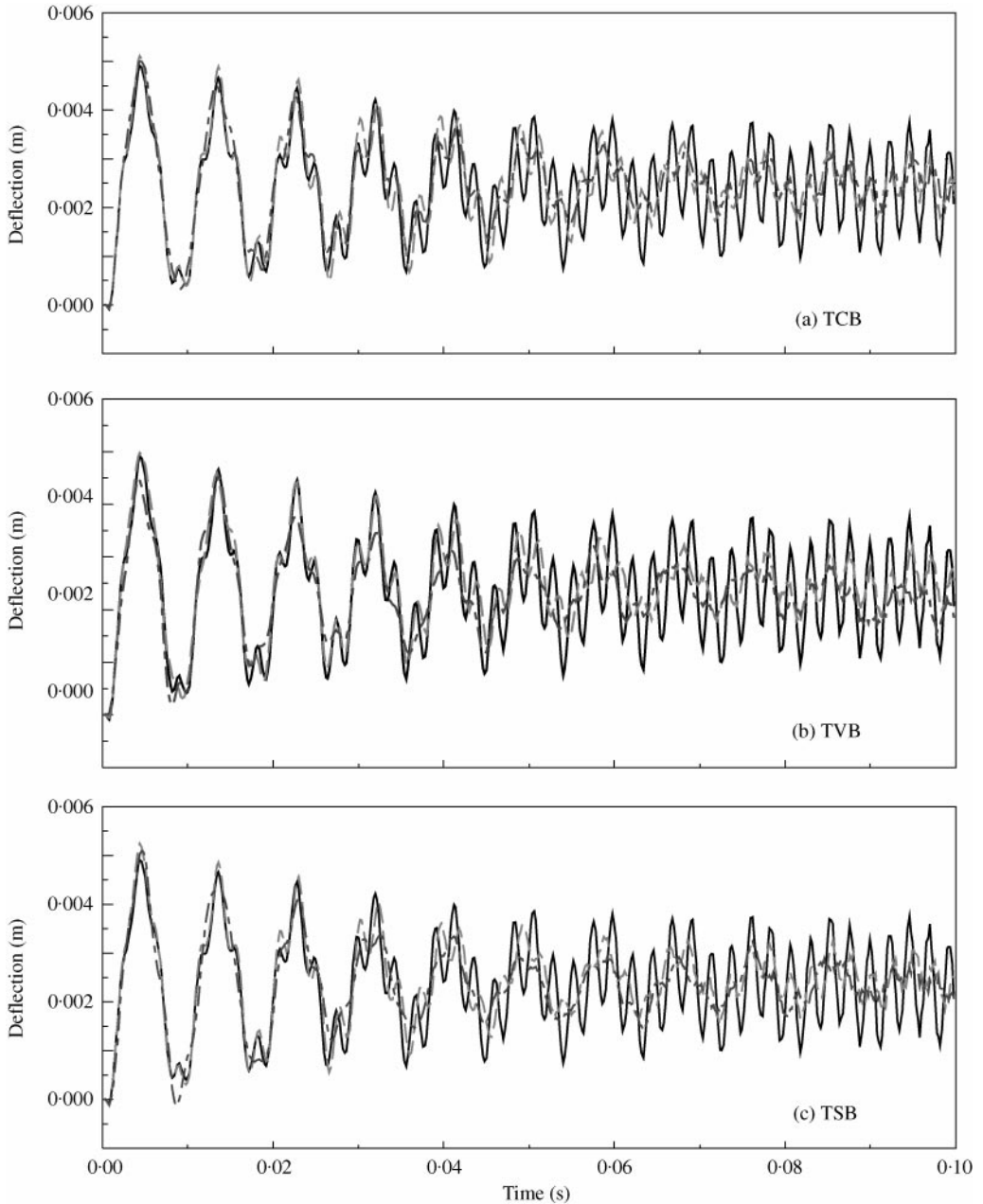
Figure 14. Effect of blowing strength on the histories of the right-tail-tip bending deflections. ——, $C_T = 0.000$; $----$ (faint line), $C_T = 0.005$; $---$, $C_T = 0.010$.

blowing directly toward the core of the leading-edge vortices has more potential in controlling the buffet loads and responses, than blowing toward the center of the wing.

Figure 19 shows the effect of blowing on the histories of the lift and drag coefficients and lift/drag ratio for the cases of rigid and flexible tails. The large transient variation present at the beginning of the time period in the rigid computations is because the rigid computations start from the undisturbed free-stream conditions, in contrast to the flexible computations
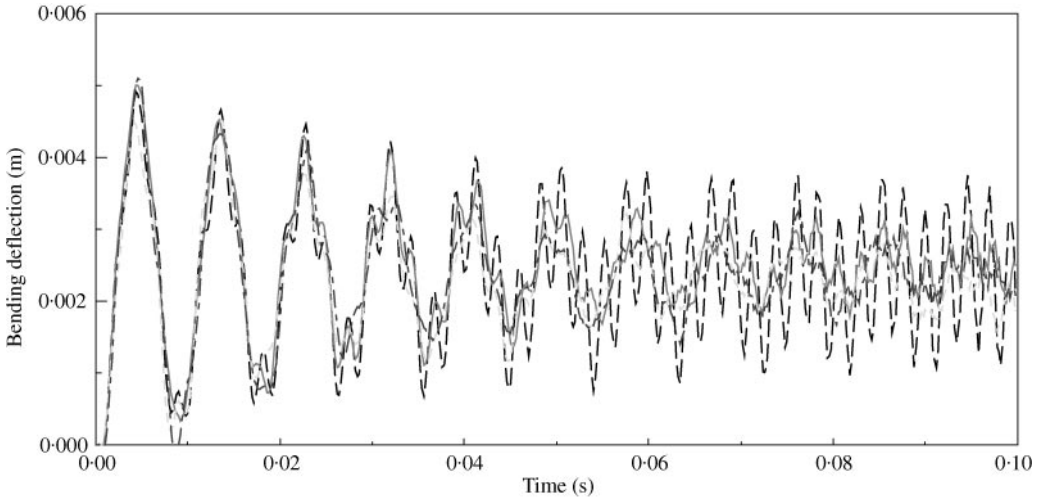
Figure 15. History of the right-tail-tip bending deflections. – – –, No blowing; ····· (faint), TCB ($C_T = 0.01$); ------ (faint line), TVB ($C_T = 0.01$); – - –, TSB ($C_T = 0.01$).
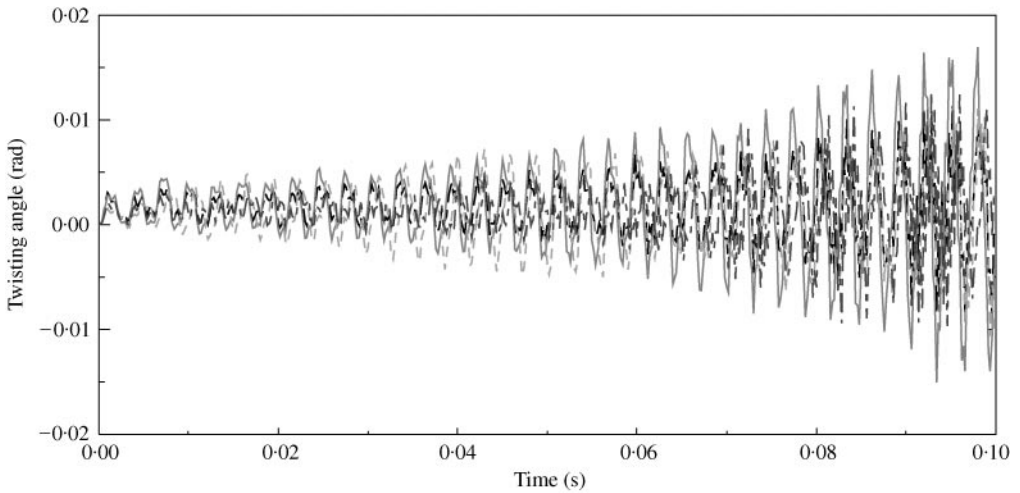
Figure 16. History of the right-tail-tip torsional deflections, – – –, No blowing; ····· (faint line), TCB ($C_T = 0.01$); ------ (faint line), TVB ($C_T = 0.01$); – - – TSB ($C_T = 0.01$).

which start from the physical initial conditions. In the case of rigid tails, the amplitudes of load oscillations are almost the same as in the case of no blowing. Any increase or decrease in the lift coefficient corresponds to an increase or decrease in the drag coefficient, respectively, resulting in almost the same lift/drag ratio. The largest reduction in the lift coefficient is about 9%. In the flexible tails case, the amplitude of load oscillation is now larger than in the case of rigid tails due to the deflection of the tail. However, the lift/drag ratio is almost the same as that of no-blowing case (less than 0·5% reduction). This figure shows the minimal effect of the proposed blowing methods on the aerodynamic characteristics of the generic fighter-aircraft configuration.
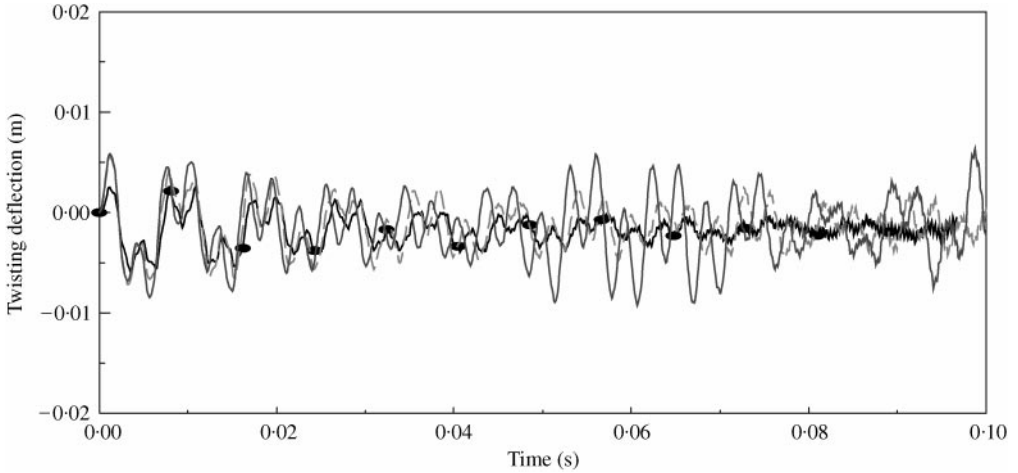
Figure 17. History of the right-tail-tip torsional deflections at different angles of attack. ●——●, AOA = 26 deg (no blowing); – – –, AOA = 34 deg (no blowing); ———, AOA = 38 deg (no blowing).
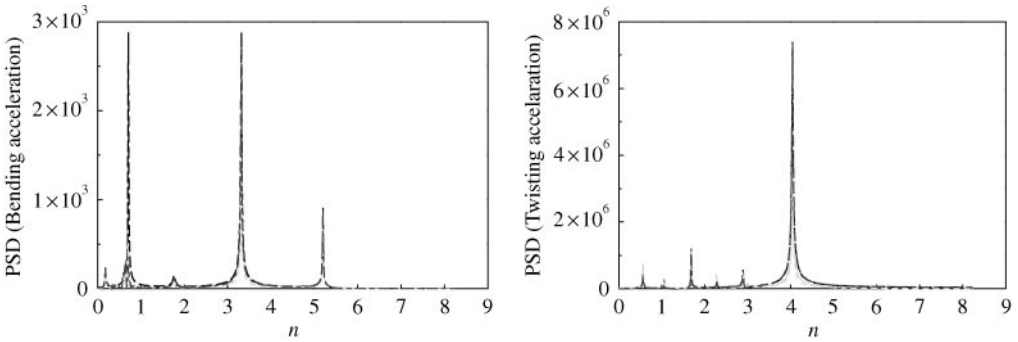
Figure 18. Power spectral density of the right-tail-tip bending and torsional accelerations. – – – –; No blowing ———, TCB ($C_T = 0.01$); - - -, TVB ($C_T = 0.01$); – – – –, TSB ($C_T = 0.01$).

4.3. COMPUTATIONAL EFFICIENCY

This complex multidisciplinary analysis of the twin-tail buffet is computed on four units of DEC ALPHA cluster of 500 MHz. The solution costs about 1 min per iteration for full Navier–Stokes computations. The same simulation costs about 3·85 min per iteration using only one DEC ALPHA 500 MHz. Therefore, a speed factor of 3·85 has been achieved using 4 units of computers, which corresponds to an efficiency of about 96%. Although the efficiency is expected to slightly decrease as the size of computer cluster increases due to the overhead cost, the speed factor is constantly increasing, which allows the fast simulation of very complex multidisciplinary problems.

5. CONCLUSION

Active vortical flow control methods by the means of tangential central blowing (TCB), tangential vortex blowing (TVB), and tangential spanwise blowing (TSB) were applied to generic fighter aircraft to alleviate the twin-tail buffet. The results indicated that the TVB and TSB methods, that blow directly into the core of the leading-edge vortices, have more potential, than any other direction, in controlling the buffet responses and in the
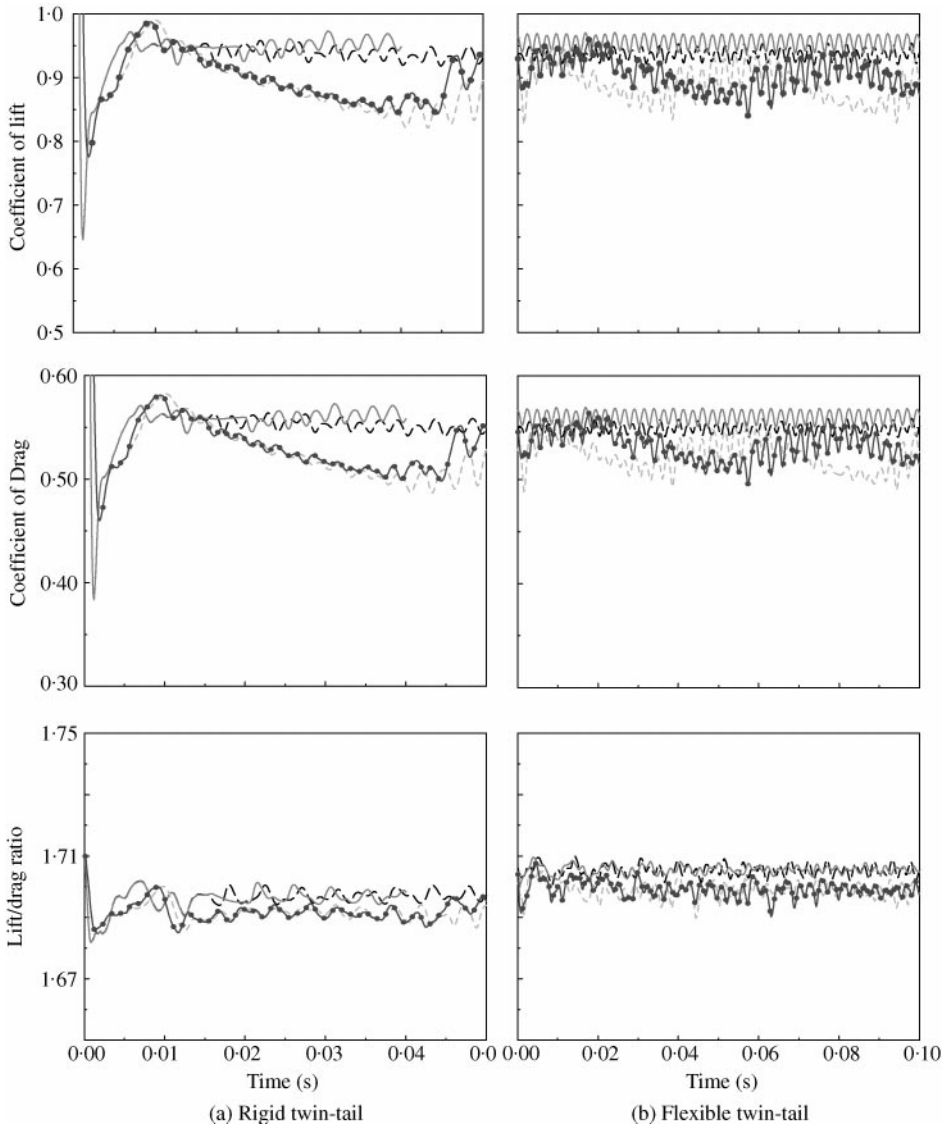
Figure 19. History of the coefficients of lift and drag, and the lift/drag ratio for the cases of rigid and flexible tails: heavy – – –, no blowing; —, TCB; light – – – –, TVB; ●—●, TSB; in all cases for $C_T = 0.01$.

reformation of unburst vortices with larger length. The TVB, in particular, produced the most favorable results with a reduction of about 43% in the buffet excitation parameter and a reduction of about 40% in the amplitude of bending deflection. Increasing the blowing strength reduced the buffet loading and responses than those achieved with low blowing strength. The flow control methods induced a minimal effect on the aerodynamic characteristics, where the lift/drag ratio was roughly the same as the no-blowing case.

ACKNOWLEDGEMENTS

REFERENCES

ANGLIN, E. L. & SATRAN, D. 1980 Effects of spanwise blowing on two fighter airplane configurations. *Journal of Aircraft* **17,** 883–889.

BROWN, S. A. 1997 Displacement Extrapolation for CFD and CSM analysis. AIAA Paper 97-1090.

CFD Research Corporation 1998 CFD-FASTRAN User's Manual. Theory Manual, Ver. 2.2.

COLE, S. R., MOSS, S. W. & DOGGET JR R. V. 1990 Some buffet response characteristics of a twin-vertical-tail configuration. NASA TM-102749.

FINDLAY, D. 1997 Numerical analysis of vertical tail buffet. AIAA Paper 97-0621-CP.

GEE, K., MURMAN, S. M. & SCHIFF, L. B. 1995 Computational analysis of F/A-18 tail buffet. AIAA Paper 95-3440-CP.

HUMMEL, D. 1978 On the vortex formation over a slender wing at large angles of incidence. AGARD-CP-247.

KANDIL, O. A. & SHETA, E. F. 1997 Coupled and uncoupled bending-torsion responses of twin-tail buffet. *Proceedings* 4*th International Symposium on Fluid–Structure Interactions, Aeroelasticity, Flow-Induced Vibration & Noise*, Vol. **3,** pp. xx–yy. New York: ASME. Also, *Journal of Fluids and Structures* **12** (1998), 677–701, doi: 10.1006/jfls.1998.0168.

KANDIL, O. A., SHETA, E. F. & MASSEY, S. J. 1996 Twin tail/delta wing configuration buffet due to unsteady vortex breakdown flow. AIAA Paper 96-2517-CP, 1136–1150.

KANDIL, O. A., SHETA, E. F. & MASSEY, S. J. 1997 Fluid/structure twin tail buffet response over a wide range of angles of attack. AIAA Paper 97-2261-CP.

KANDIL, O. A., YANG, Z. & SHETA, E. F. 1999 Flow control and modification for alleviating of twin-tail buffet. AIAA Paper 99-0138.

KINGSLEY, G. M., SIEGEL, J. M., HARRAND, V. J., LAWRENCE, C. & LUKER, J. 1998 Development of the Multi-Disciplinary Computing Environment (MDICE). AIAA Paper 98-4738, 7th AIAA/USAF/ NASA/ISSMO Symposium of MDO.

LEE, B., BROWN, D., ZGELA, M. & POIREL, D. 1990 Wind tunnel investigation of tail buffet on the F-18 aircraft. AGARD CP No. 483, Paper 1.

LEE, B. & VALERIO, N. 1994 Vortical-flow structure near the F/A-18 LEX at high incidence. *Journal of Aircraft* **31,** 1221–1223.

MARTIN, C. A. & THOMPSON, D. H. 1991 Scale model measurements of fin buffet due to vortex bursting on F/A-18. AGARD CP-497.

MEYN, L. A. & JAMES, K.D. 1993 Full scale wind tunnel Studies of F/A-18 tail buffet. AIAA Paper 93-3519-CP.

MILLER, L. S. & GILE, B. E. 1993 Effects of blowing on delta wing vortices during dynamic pitching. *Journal of Aircraft* **30,** pp. 334–339.

MORTON, S. A., RIZZETTA, D. P. & MELVILLE, R. B. 1998 Numerical simulation of the interaction between a leading-edge vortex and a flexible vertical tail. AIAA Paper 98-1957.

RIZK, Y. M., GURUSWAMY, G. P. & GEE, K. 1992 Numerical investigation of tail buffet on F-18 aircraft. AIAA Paper 92-2673-CP.

SEGINER, A. & SALOMON, M. 1986 Performance augmentation of a 60-degree delta aircraft configuration by spanwise blowing. *Journal of Aircraft* **23,** 801–807.

SELLERS III W. L., MEYERS, J. F. & HEPNER, T. E. 1988 LDV survey over a fighter model at moderate to high angle of attack. SAE Paper 88-1448.

SHAH, G. H. 1991 Wind-tunnel investigation of aerodynamic and tail buffet characteristics of leading-edge extension modifications to the F/A-18. AIAA Paper 91-2889.

SHETA, E. F. 1998 Computational investigation and validation of twin-tail buffet response including dynamics and control. Ph.D. dissertation, Old Dominion University, Norfolk, VA, U.S.A.

SHETA, E. F. 2000 Prediction and control of twin-tail buffet of fighter aircraft. Final Report, SBIR Phase I, Contract No. F33615-99-C-3213, US Air Force Research Laboratory.

SHETA, E. F. & KANDIL, O. A. 1999 Effect of dynamic rolling oscillations on twin tail buffet response. AIAA Paper 99-0792.

SHETA, E. F., KANDIL, O. A. & YANG, Z. 1998 Effectiveness of flow control for alleviation of twin-tail buffet. WAC Paper No. 985501, SAE-AIAA World Aviation Congress and Exposition, Anaheim, CA, U.S.A.

SHETA, E. F., SIEGEL, J. M., GOLOS, F. N. & HARRAND, V. J. 1999 Twin-tail buffet simulation using a Multi-Disciplinary Computing Environment (MDICE). NASA/CP-1999-209136, 627–643, CEAS/AIAA/ICASE/NASA Langley IFASD, Williamsburg, VA, U.S.A.

SIEGEL JR J. M., PARTHASARATHY, V., KINGSLEY, G. M., DIONNE, P. J., HARRAND, V. J. & LUKER, J. J. 1998 Application of a multi-disciplinary computing environment (MDICE) for loosely coupled fluid– structural analysis. AIAA Paper 98-4865, 7th AIAA/USAF/NASA/ISSMO Symposium of MDO.

THOMPSON, J. F., SONI, B. K. & WEATHERILL, N. P. 1998 Handbook of Grid Generation. Boca Raton, FL: CRC Press.

WASHBURN, A. E., JENKINS, L. N. & FERMAN, M. A. 1993 Experimental investigation of vortex–fin interaction. AIAA Paper 93-0050.

WENTZ, W. H. 1987 Vortex–fin interaction on a fighter aircraft. AIAA Paper 87-2474.

WONG, G. S., ROCK, S. M., WOOD, N. J. & ROBERTS, L. 1994 Active control of wing rock using tangential leading-edge blowing. *Journal of Aircraft* **31,** 659–665.

WOOD, N. J. & ROBERTS, L. 1988 Control of vortical lift on delta wings by tangential leading-edge blowing. *Journal of Aircraft* **25,** 236–243.